JEPECS
Journal of Electric Power and Energy Conversion Systems

JOURNAL OF ELECTRIC POWER AND ENERGY CONVERSION SYSTEMS (JEPECS)
JEPECS VOL. 1, NO. 3, PP. 127-134, AUTUMN 2016
ISSN: 2345-4830 print/2345-4733 online

Optimal Control of A Variable-Speed Wind Energy Conversion System: A New Approach

Ali Mohammadi,* Saeed Tavakoli,†

The operation of wind energy conversion systems mainly deals with variable and unpredictable wind regimes resulting in variable power efficiency. In addition, nowadays with the presence of high penetration level of wind farms integrated to power systems, stability and power quality problems might be addressed, when a disturbance event occurs. These challenges are worsened with significant degree of nonlinearity, which leads to complex control. In this research despite common sophisticated methods, a novel control strategy based on linear controllers were employed to guarantee sufficient damping and performance once it undergoes the test including power regulation, wind speed variation and voltage sag and swell. Furthermore, a new optimal linearization technique was proposed to improve accuracy in comparison with conventional linearization methods. The simulation results on a full variable-speed benchmark system show the effectiveness of the optimized methods in the fulfilment of the control requirements within an acceptable time in terms of relevant control indices.

Keywords:Variable Wind System, Control Design, Linear Control, Power Quality.

Received Nov. 2016; Revised Feb. 2017; Accepted March 2017.

NOMENCLATURE

Ψ_{qs}, Ψ_{ds}	the q-axis and d-axis flux of the stator
Ψ_{qr},Ψ_{dr}	the q-axis and d-axis flux of the rotor
ω_e,ω_r,ω_b	angular speed of the synchronous reference frame, rotor angular speed and base angular speed
v_{qs}, v_{ds}	q-axis and d-axis voltage of the stator
X_{ls},X_{lr},X_M	the stator leakage, rotor leakage and magnetizing reactances
r_s,r_r	the stator and rotor resistance
ω_o, ω_i	reference frame frequency of grid side converter, and generator side converter
i_{qi}, i_{di}	currents of generator side converter
i_{qo}, i_{do}	currents of grid side converter
U_d	capacitor voltage
v_{qi}, v_{di}	input voltages of generator side converter
v_{qin}, v_{din}	voltages of generator side converter
v_{qo}, v_{do}	output voltage of grid side converter
v_{qou}, v_{dou}	voltages of grid side converter
A_{mi}, α_{mi}	amplitude and angle modulation indices of generator side converter
A_{mo}, α_{mo}	amplitude and angle modulation indices of grid side converter
ω_t,ω_g	the turbine and generator speed
T_s,T_t,T_e	the internal shaft, the turbine and generator torques
D_t,D_g,D_s	the damping coefficients of the turbine, generator and shaft
K_s,n	the shaft stiffness and the gearbox ratio
ρ_{air}, R, β	the air density, the rotor radius and pitch angle
A_r,v_w, λ	the area swept by rotor blades, wind speed and tip speed ratio
v_{m},L,σ	the average wind speed, turbulence length and standard deviation of the wind speed

I INTRODUCTION

In recent years, wind energy has been considered an alternative choice to make up a significant proportion of power grids in developed countries with high wind potential [1]. However, investors, designers and operators in the wind industry could face a number of limitations and difficulties, especially once wind systems are integrated to the universal power system [2]. The main challenge of wind farms is the variable nature of this type of energy in terms of geographical and climatic situations [1]. Hence, power captured from wind turbines could generally undergo changes in sympathy with the wind profile. Another important concern is the effect on power quality, most of which stems from the variable wind speed and its turbulent components [3]. As a result, power electric companies have made tight regulations on wind power quality according to IEC and IEEE standards to confine power quality distortions. Since the installation of the first commercial wind energy conversion system (WECS), stability issues have been taken into account by wind specialists [1]. Therefore, this attitude towards wind systems led to consideration into voltage support and the definition of concepts regarding the stability of a wind system, such as low voltage ride through [3]. But, what requires wind experts to revise their planning programs is high penetration of wind farms in a power system in comparison with conventional power generation units[3]. Accordingly, not only does a change in the operating points of a wind system has a serious impact on the power transmitted to the grid, but also it could offset critical grid variables and as a cascaded result network red lines might be violated [4].

In addition, it is made more complex to control highly nonlinear wind systems, significant amount of which is due to the nonlinear wind turbine model [5]. As a consequence, there have been a variety of complicated control strategies [6-17] to mitigate their notable level of nonlinearity so that a wind different operating points. Mostly, the perturbation about a nominal equilibrium point is made by [1]: (a) change in reference power controlled by the transmission system operator (b) change in wind speed and (c) voltage variation including sag and swell voltage.

On this account, the center of this study has been assigned on

*MSc Other +989153522693 Department of Electrical Engineering, Faculty of Electrical and Computer Engineering, University of Sistan and Baluchestan, ali.mohammadi2693@gmail.com

†PhD Associate Professor +985431136556 Department of Electrical Engineering, Faculty of Electrical and Computer Engineering, University of Sistan and Baluchestan, tavakoli@ece.usb.ac.ir (corresponding author)

the control of active and reactive power injected by a variable wind system in response to the changes above in order that under (a) the power signal must track the desired commands and on the contrary, the power oscillation resulted from (b) and (c) is required to be mitigated effectively. The case study is a full variable-speed wind system with a squirrel-cage induction generator driven by an active-stall wind turbine, which is connected to a definite bus.

A number of studies were dedicated to nonlinear control methods [6-13]. For example, sliding mode control [10], [11] and backstepping technique [12], [13] were extensively employed. Moreover, others worked on soft computing-based control algorithms [14-17], say neural networks [16, 17] and adaptive network fuzzy inference system (ANFIS) [14, 15]. In these literatures, what is implied in the same manner is the lack of practically easy implementation and the added degree of nonlinearity imposed by the controller, which was considered to cope with initially nonlinear wind system. Therefore, the first step to reduce complexity in control design was taken to look for regulators with fluent implementation and fine tuning. Firstly, according to [18], linear strategies were singled out. Nevertheless, experience of using linear methods questions their effectiveness compared to complex schemes. In several projects, it was reported that linear controllers resulted in weak performance at various operating points [19, 20].

On the other hand, without loss of generality, this study tackled the augmentation of linear controllers to operate as efficiently as a complex method. From control perspective, damping, and performance are factors justifying complex control in wind systems. Hence, a novel control algorithm was proposed to incorporate three control objectives into the controller design to boost a linear controller. The linearized model of a wind system with conventional methods was questioned by [21]. To remedy this situation, a new linearization technique through an optimal approach was adopted to obtain acceptable approximation.

In all simulations of this research, following assumptions have been made: 1. Magnetic saturation of electric machines is neglected 2. The distribution of magnetic flux is sinusoid 3. Any losses except copper loss are neglected 4. All voltages and currents in the whole power system at the synchronous frequency is sinusoid

The outline of this report is organized as follows. Section II is dedicated to modeling. In section III, the linearization technique is explained. Next, the novel control strategy is proposed in section IV. Finally, the simulation results and discussion are included in section V.

II MODELING

Evaluation of the controller performance depends greatly on a valid model representation. Not only obtained model should be precise enough, but also it should neglect dynamics of the low participation in system performance to reduce computations and the total simulation time appropriately. Configuration of WECS under study is a single machine infinite bus (SMIB) (Fig. 1), including the variable speed wind turbine, the squirrel-cage induction generator, and a drive train. An SFC is utilized to control active and reactive power independently through the variable pitch turbine and the power electronics converter. The back-back pulse width modulation (PWM) voltage-source converter of the full power type is also employed to supply the required transferred reactive power into both generator and grid to have an acceptable power flow, as well as to decouple the generator frequency and grid frequency.

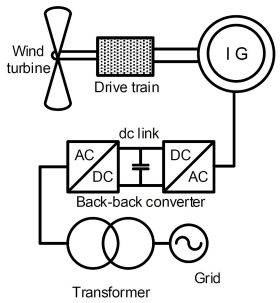

Figure 1: Wind system under study

A Induction generator

The dynamic aligns governed by the induction machine can be written in a synchronously rotating d–q reference frame as follows [22]:

$$\dot{\Psi}_{qs} = -\omega_b \frac{r_s X_{rr}}{D}\Psi_{qs} - \omega_e \Psi_{ds} + \omega_b \frac{r_s X_M}{D}\psi_{qr} + \omega_b v_{qs} \quad (1)$$

$$\dot{\Psi}_{ds} = \omega_e \Psi_{qs} - \omega_b \frac{r_s X_{rr}}{D}\Psi_{qs} + \omega_b \frac{r_s X_M}{D}\psi_{dr} + \omega_b v_{ds} \quad (2)$$

$$\dot{\Psi}_{qr} = \omega_b \frac{r_r X_M}{D}\Psi_{qs} - \omega_b \frac{r_r X_{ss}}{D}\Psi_{qr} - (\omega_e - \omega_r)\,\psi_{dr}, \quad (3)$$

$$\dot{\Psi}_{qr} = \omega_b \frac{r_r X_M}{D}\Psi_{ds} + (\omega_e - \omega_r)\,\Psi_{qr} - \omega_b \frac{r_r X_{ss}}{D}\psi_{dr} \quad (4)$$

where $X_{ss} = X_{ls} + X_M; X_{rr} = X_{lr} + X_M; D = X_{ss}X_{rr} - X_M^2$.

WIND TURBINE MODEL

Output mechanical power by the turbine is calculated by;

$$P_t = \frac{1}{2}\rho_{air} A_r V_w^3 C_p\,(\lambda, \beta) \quad (5)$$

where C_p is the power coefficient of the turbine which is a function of pitch angle (β) and $\lambda = \frac{\omega_t R}{v_w}$, the tip speed ratio, and. Estimation of C_p for the active-stall turbine under study is given by [23]

$$C_p(\lambda, \beta) = (0.44 - 0.0167\beta)\sin\left(\frac{\pi\,(-3+\lambda)}{15 - 0.3\beta}\right) - 0.00184(-3+\lambda)\beta. \quad (6)$$

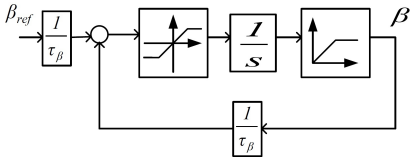

Figure 2: Pitch control model

It is observed from (**??**) that output power is controllable by variable pitch angle. The pitch mechanism is represented as a first-order system, considering the amplitude and rate limiters of the pitch [22] (Fig. 2). A hydraulic pitch actuator with $\beta \in [-2, 30]$ and a rate limit of $\pm 10°$/s is used in this paper [24]. And β_{ref} is the pitch set point and τ_β is the integral time constant.

A practical wind model is indispensable for a comprehensive evaluation of the controller performance. One approach to represent wind speed is defined by the supervision of four components: average value, a ramp component, a gust component, and turbulence component [25]. The simulation is performed in the time domain whilst the turbulence component is defined as a power spectral density in the frequency domain; thus the conversion of frequency domain value into a time sequence is complex. Another approach describes the wind speed as a random process based on a generic model that is a power spectral density, as [26]

$$v_w = A_0 + \sum_{i=1}^{N} A_i \cos(\omega_i t + \varphi_i) \tag{7}$$

$$\mathrm{S}(\omega) = \frac{0.475\sigma^2 \frac{\mathrm{L}}{\mathrm{v_m}}}{\left[1 + \left(\frac{\omega \mathrm{L}}{\mathrm{v_m}}\right)^2\right]^{\frac{5}{6}}} \tag{8}$$

Most common models for s_{vv} are the Van der Hoven, the Kaimal, and the von Karman [26]. The von Karman represents more realistic model for the turbulence component in wind tunnels [26]. The von Karman spectrum, consequently, is employed in this work which is given by align (**??**) [27].

Once wind passes across the turbine components, a high frequency variation is experienced by the rotor surface. This effect is modelled as a low pass filter given by $H_w = \frac{1}{1+\tau S}$., [28,29].

DRIVE TRAIN MODEL

There are four common models for the drive train: six-mass model, three-mass model, two-mass shaft model and single mass model. The six-mass model considers three blade inertias, hub inertia, gearbox inertia, and generator inertia [30]. In the three-mass model, the turbine inertia is obtained from the combined weight of the blades and hub. Two mass model is represented by connecting two disks including equivalent shaft stiffness as well as neglecting the gearbox inertia [30-32]. To represent the single-mass model, all components of the drive train are lumped together. High-order models are not proper for large power systems studies. Thus, a reduced model with acceptable accuracy is preferred. The dominant lowest frequency mode is principal [1] and the resonance modes associated with gearbox and high-speed shaft typically lie beyond the frequency bandwidth defined in power system dynamics [31]; hence, the two-mass model (Fig. 3), which incorporates the lowest frequency component and assumes that both the high speed shaft and gearbox are indefinitely stiff., is suitable.

Two-mass model takes into account the inertias of the low speed turbine and the high speed generator and models the connected shaft as springs and dampers. The differential aligns of two-mass model can be expressed as

$$\dot{\omega}_t = \tfrac{1}{J_t}\left(T_t - T_s - D_t\omega_t\right) \tag{9}$$

$$\dot{\omega}_g = \tfrac{1}{J_g}\left(-T_e + \frac{T_s}{n} - D_g\omega_g\right) \tag{10}$$

$$\dot{T}_s = K_s\left(\omega_t - \frac{\omega_g}{n}\right) + D_s\left(\dot{\omega}_t - \dot{\omega}_g\right) \tag{11}$$

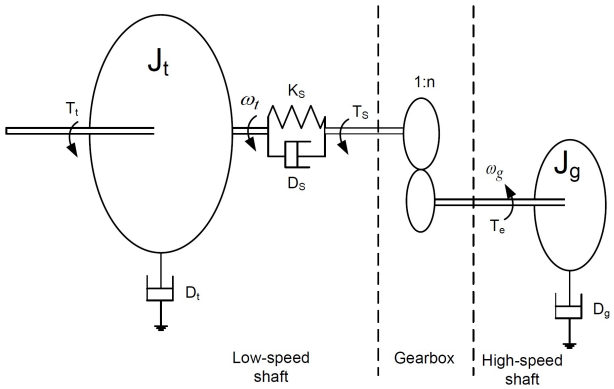

Figure 3: Drive train model

Converter model

Fig. 4-a depicts a single-line diagram of the employed converter. The converter model can be written in the synchronous d-q reference frame (Fig. 4-b) as follows [33]:

$$\dot{i}_{qi} = \frac{1}{L_i}\left[-R_i i_{qi} - L_i\omega_i i_{di} + v_{qi} - v_{qin}\right] \tag{12}$$

$$\dot{i}_{di} = \frac{1}{L_i}\left[-R_i i_{di} + L_i\omega_i i_{qi} + v_{di} - v_{din}\right] \tag{13}$$

$$\dot{i}_{qo} = \frac{1}{L_o}\left[-R_o i_{qo} - L_o\omega_o i_{do} - v_{qo} + v_{qou}\right] \tag{14}$$

$$\dot{i}_{do} = \frac{1}{L_o}\left[-R_o i_{do} + L_o\omega_o i_{qo} - v_{do} + v_{dou}\right] \tag{15}$$

$$\dot{v}_d = \frac{1}{C}\frac{3}{4}\left[i_{qin} + i_{din} - i_{qou} - i_{dou}\right] \tag{16}$$

For the grid side, voltage-oriented vector control is employed to align the grid side reference frame with SMIB voltage. Furthermore, the phase of flux stator is the origin of the flux-oriented control for the generator side. Therefore: $\theta_i = \angle\Psi_s$, $\theta_o = \angle V_{ou}$.

The instantaneous active and reactive power at the grid bus can be calculated as, $P_g = \frac{3}{2}\left(v_{do}i_{do} + v_{qo}i_{qo}\right)$, $Q_g = \frac{3}{2}\left(v_{qo}i_{do} - v_{do}i_{qo}\right)$.

III LINEARIZATION

For a systematic control strategy, the overall dynamic aligns are linearized around the nominal operating point as

$$\begin{aligned} \Delta\dot{x} &= A'\Delta x + B'\Delta u \\ \Delta y &= C'\Delta x + D'\Delta u \end{aligned} \tag{17a}$$

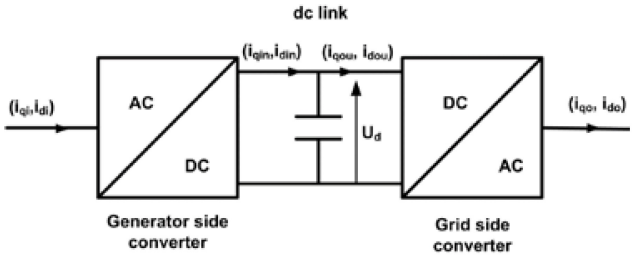

(a) two-level voltage source converter

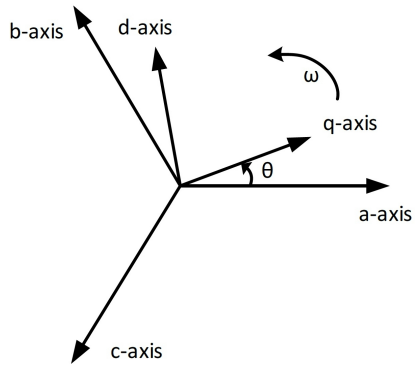

(b) Synchronous reference frame

Figure 4

where the state vector, control input vector, the disturbance input vector and the output vector are as follows:

$$x=\begin{bmatrix}\Psi_{qs} & \Psi_{ds} & \Psi_{qr} & \Psi_{dr} & i_{qo} & i_{do} & v_d & \omega_r & \omega_t & T_s & \beta\end{bmatrix}^T \tag{17b}$$

$$u=\begin{bmatrix} u_c & u_d \end{bmatrix}^T$$

$$u_c=\begin{bmatrix} A_{mi} & \alpha_{mi} & A_{mo} & \alpha_{mo} & \omega_o & \beta_{ref} \end{bmatrix}^T \tag{17c}$$

$$u_d=v_w$$

$$y=\begin{bmatrix} P_g & Q_g \end{bmatrix}.^T \tag{17d}$$

It is worth mentioning, the electrical power is regulated by the converter through the modulation indices and the mechanical power is conditioned by variable pitch angle and the grid side frequency. Hence, the controller incorporates these control inputs together to track active and reactive power set points properly (Fig. 5-a). It is pointed out that the equilibrium point has been obtained by a sequential quadratic programming (SQP) algorithm in terms of the desired values [21] as tabulated in Table 1, where superscript "0" denotes the operating point. Small-signal analysis for the linearized system disclosed that eigenvalues around the equilibrium point include negative real part; thus asymptotical stability of the system is verified ı (Table 2).

To make sure the obtained linearized model is an appropriate alternative to the actual system, it must be validated by a comparison of its response to a certain input signal so that the worst case would be taken into consideration. As the step input signal has a discontinuity at the start point and covers a wide range of frequencies, this signal was selected as a benchmark test. Consequently, several validation simulations were run for each control input as indicated in Table 3.

Fig 5-b. Shows the reaction of the outputs to the corresponding inputs, where red and blue waveforms apply to linearized and actual wind system. The results confirm acceptable approximation except the input Ami. This significant mismatch is due to ignoring high-order terms in Taylor's series and high amount of nonlinearity. To surmount this obstacle, an optimal linearization method is proposed as below.

Because the error problem was just seen in response to an input, it is enough to decouple the dynamic align of that input-output coordination from the rest. The state aligns could be described that minimizes the following error objective function: $F_e = Max\left(|y_L - y_N|\right)$ where Y_L,Y_N are the output of linearized and actual systems at time t. In this study genetic algorithm (GA) is employed to solve this optimization problem. The post-optimization simulation results (Fig. 5-b) revealed that the obtained linearized model by the proposed method has a reasonable approximation of tracking the actual system.

Table 1: Calculated equilibrium points

Input	***Value***	***State***	***Value***
$\omega_{\rm o}^0$[*rad/sec*]	376.9099	$\Psi_{\rm qs}^0[v]$	-3288.57
A_{mo}^0	0.797357	$\Psi_{ds}^0[v]$	76.92566
$\alpha_{\rm o}^0$[*deg*]	0.007266	$\Psi_{\rm qr}^0[v]$	-3215.28
A_{mi}^0	0.800017	$\Psi_{\rm dr}^0[v]$	116.1775
$\alpha_{\rm i}^0$[*deg*]	-0.12706	$\rm i_{qg}^0[A]$	7.855352
$\beta_{\rm ref}^0$[*deg*]	-0.04534	$\rm i_{dg}^0$[A]	-15.3288
$\rm v_w^0$[*m/sec*]	9.928041	$\rm v_d^0$[v]	8203.878
Output	***Value***	$\omega_{\rm t}^0$[rad/sec]	9.432152
$\rm P^0$[kW]	75.09548	$\omega_{\rm r}^0$[rad/sec]	377.2861
$\rm Q^0$[kVar]	38.48321	$\rm T_s^0$[N.m]	8791.349
		β^0[deg]	-0.04534

Table 2: Small-signal stability

Eigenvalues at the operating points	
-4929.125 ± 9809.386 j	-3.449346 ± 65.18479 j
-9987.934	-27.79234
-285.1776 ± 358.4156 j	-2
-28.05782 ± 140.5585 j	

Table 3: Step input for validation

ω_o	$\rm A_{mo}$	$\alpha_{\rm mo}$	$\rm A_{mi}$	$\alpha_{\rm mi}$	β_{ref}	v_w
1	0.1	30	0.1	0.1	30	1

IV CONTROLLER DESIGN

To achieve the zero steady-state error (zero for active power Pg and reactive power Qg), those integral terms, which are the most relevant to the error reduction, are necessary to be augmented to the state variables to the entire state variables as well as those defined in (17-b) [34]; then the controller is designed for the augmented system (Fig. 6).

The operating point changes as a result of the input disturbances, such as the wind speed; thus the variable output set points and

rejecting the disturbance inputs are essential. To obtain sufficient damping for ΔP_g and ΔQ_g as well as guarantee tight regulation of $\delta P_g = P_g^* - P_g$ and $\delta Q_g = Q_g^* - Q_g$, in this work, integral terms of $\int \delta P_g dt$ and $\int \delta Q_g dt$ are augmented to the state variables. Subsequently, the augmented representation is described as

$$\Delta \dot{x}_a = A'_a \Delta x_a + B'_a \Delta u + B'^*_a \Delta u^*$$
$$\Delta y_a = C'_a \Delta x + D'_a \Delta u + D'^*_a \Delta u^* \quad (18)$$

where the augmented state vector, augmented input set point vector, augmented output vectors, and the corresponding matrices are given in [35].

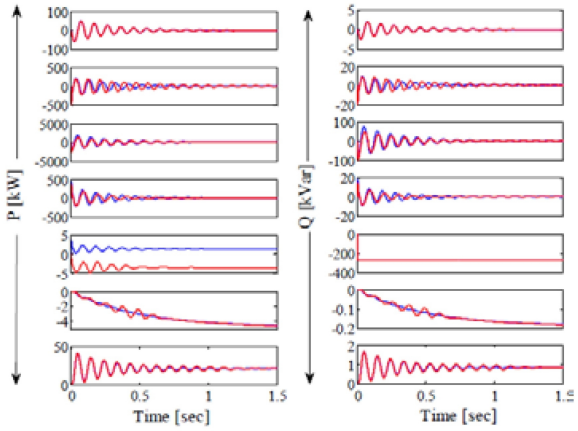

(a) Linearization by conventional method

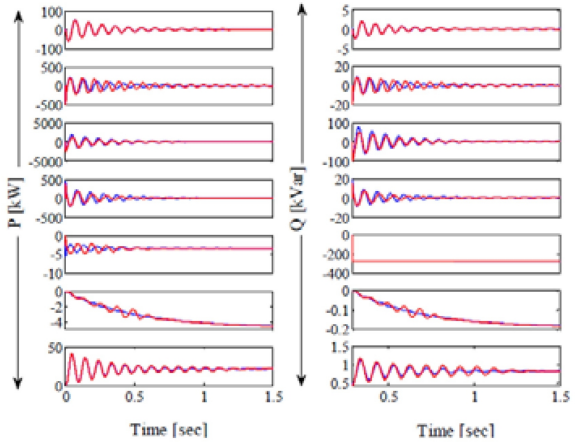

(b) Linearization by the proposed technique

Figure 5

For the augmented model, the control signal of the state feedback is obtained by minimizing the linear quadratic cost function, with output weighting, as [27]

$$J = \int_0^\infty (\Delta y_a^T Q \Delta y_a + \Delta u^T R \Delta u) dt \quad (19a)$$
$$\Delta u_{op} = -R^{-1} B^T M_s \Delta x_a = -K_{op} \Delta x_a \quad (19b)$$

where $Q \geq 0$ and $R > 0$ are the output and input weighting matrices; then the optimal control effort is given by the align

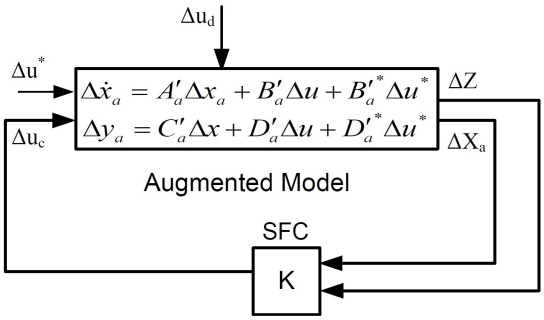

Figure 6: Controller structure

(19b). where matrix $M_s > 0$ is the solution to the Riccati align as

$$A_a^T M + M A_a - M B_a R^{-1} B_a^T M + Q = 0. \quad (19c)$$

It has been shown in the literature that the performance of LQ controller is cling to the choosing of the weighting matrices [27]. Furthermore, there is no certain align to express the performance objectives, i.e. maximum overshoot ($P.O$), maximum undershoot ($P.U$) and settling time (t_s), in terms of Q and R. Hence, the control design deals with optimal selection of weighting matrices to achieve the optimal LQC and meet the performance requirements as well. Common approach is based on the Baryon's rule by which each term in (19a) is scaled. The Bryson's rule cannot assure tight performance specifications sufficiently; thus this rule is often used as a start point to a trial-and-error method. WECS under study is MIMO; therefore, the iterative method should be systematic and intelligent enough to obtain the desired performance. A new iterative approach is proposed in the following section.

In the selection of Q and R, another performance index is chosen to express the desired specifications properly and, designate equal weighting factors between the transient and steady-state response from a behavior assessment point of view. Hence, integral absolute error (IAE) is employed, in this study. Meanwhile, the control objective should take into account the worst-case error; thus maximum IAE of the outputs, which have been well-scaled, is considered the performance objective given by

$$F = \max_{Q,R} \left\{ \int_0^\infty |\delta(\bar{y}_i)|\, dt \right\}, \quad (20a)$$
$$\text{subject to} \quad \begin{matrix} P.O < P.O^{cr} \\ P.U < P.U^{cr} \\ t_s < t_s^{cr} \end{matrix} \quad (20b)$$

where $\bar{y}_i$ is the ith well-scaled output and superscriptcrdenotes critical bounds, which were opted 10% and 5 sec for $P.O^{cr}$ and t_s^{cr} respectively. Consequently, with the aid of this new index, a reasonable performance evaluation SFC is acquired as shown in Fig. 7.

First, matrices Q and R are initialized using the Bryson's rule; then the state feedback gain and thus the control effort is obtained by solving the Riccati align. Once the resultant solution satisfies the performance specifications, the algorithm will ter-

minate the iterative procedure and the solution is valid; otherwise another solution for Q and R is iteratively to be generated to evaluate it as described above. This iterative generation of the efficient solution is performed by minimizing the new index in (20a); having the initial point from the first iteration, this non-explicit optimization problem is solved using GA. An overview of the proposed approach is demonstrated in Fig. 8 This iterative optimization is carried out until the optimal solution produced by GA, is converged at as acceptable speed as over 31 iterations (Fig. 9)...

V Simulation results and discussion

To evaluate the performance of the proposed controller, three simulations with different conditions are carried out all of which the control or disturbance input signal has been applied at t=0.5 sec. The first simulation included set point tracking, where the incremental set point value of the active power is set to 30% and the reactive power to 15%. Active power response is over-damped as $ts = 0.0014s$ (Fig. 10-a(a)) and reactive power is settled down with $P.O = 2.4\%$ and $ts = 0.0016s$ (Fig. 10-a(b)). As a result, link-dc voltage is reduced by 84.74% (Fig. 10-a(c)). The generator speed which, has an inverse response with minimum variation of 0.9583 rad/s, is reduced by 1.825 rad/s (Fig. 10-a(d)).

In the second scenario, the wind speed is increased to 2 m/s. With this wind speed variation, generator speed is increased (Fig. 10-b(d)). This disturbance results in, transiently, a reduction swing of 32.63% in active power; therefore $P.U = 4.4\%$ as depicted in Fig. 10-b(a) and two successive swings of +0.493% and -0.338% in the variations of reactive power, i.e., $P.O = 1.28\%$ and $P.U = 0.88\%$ as illustrated in Fig. 10-b(c). After WECS meets the controller damping, active and reactive power are properly damped. Consequently, reduction of generator speed by 1.19% (Fig. 10-b(d) and 59.22% increase of dc-link voltage (Fig. 10-b(c)) are observed.

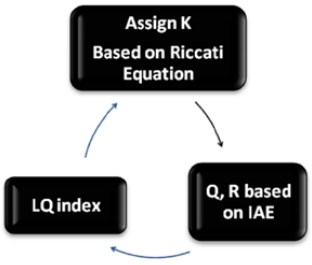

Figure 7: Controller assessment

The last scenario is 50% sag of grid voltage. First of all, active power and reactive power are slightly oscillated as the increase and decrease of 0.005%, respectively, as shown in Fig. 10-c(a) and (b). Active power is given $P.O = 0.0078\%$ and $P.O = 0.0011\%$ and $P.U = 0.0135\%$ are calculated for reactive power; after that, WECS outputs are settled to the nominal values. Meanwhile, as seen in Fig. 10-c(c) and d, this rejection causes generator speed variation of $+0.032\%$ and that of capacitor voltage by -0.06958%. The performance specifications of the proposed controller are shown in Table 4. Maximum values

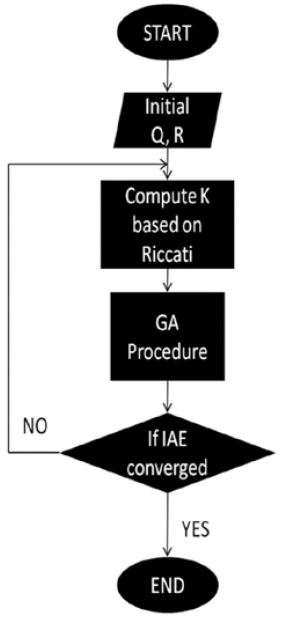

Figure 8: Flowchart of the proposed control algorithm

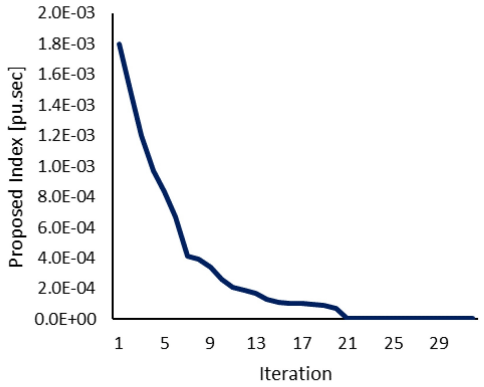

Figure 9: convergence speed of the porposed index opitmization by GA

of active and reactive power are 0.0078% and 2.10%. The most $P.U$ associated with inverse response, are obtained as 0.8765% and 4.4064%. The longest t_s is calculated as 0.0015 and $0.016s$. Ultimately, it is deduced that the proposed controller is managed to regulate outputs effectively in response to set point variation and rejection of the disturbances so that not only the resultant responses are as rapid as possible are suitably damped, but also the bounds of the performance specifications are satisfied according to 25b

Table 4: Evaluation of the controller performance. (a) set point tracking (b) wind speed mitigation (c) voltage sag mitigation

Goal	Controlled	P.O [%]	P.U [%]	t_s [s]
(a) Set point tracking	Pg	-	-	0.0014
	Qg	2.402	-	0.0016
(b) Wind speed rejection	Pg	-	4.4064	0.0014
	Qg	1.2814	0.8765	0.0017
(c) Voltage sag rejection	Pg	0.0078	-	0.0015
	Qg	0.0011	0.0135	0.0019

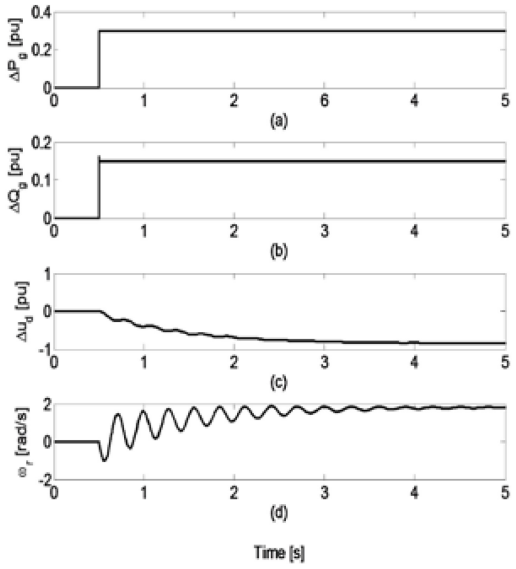

(a) Dynamic responses for increase of 30% in p* and 15% in q*. (a) grid active power (b) grid reactive power (c) dc-link voltage (d) angular speed of IG

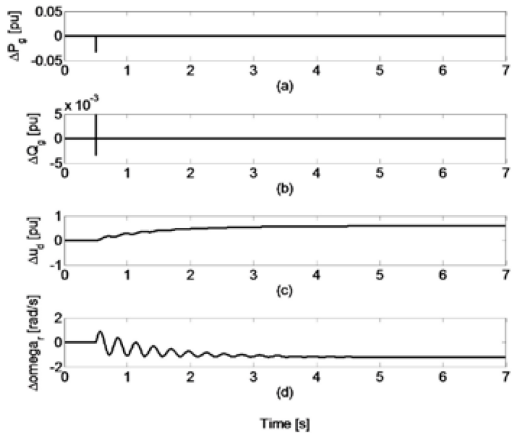

(b) Dynamic responses under increase of 10% in vw. (a) grid active power (b) grid reactive power (c) dc-link voltage (d) angular speed of IG

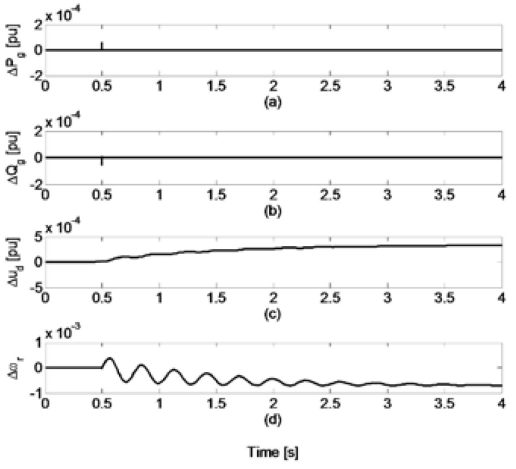

(c) Dynamic responses under 50% sag of grid voltage. (a) grid active power (b) grid reactive power (c) dc-link voltage (d) angular speed of IG.

VI Conclusion

A novel control strategy was designed to resolve the common problems of wind systems. Variable wind speed, power quality problems must be damped appropriately. On the other hand, a wind system is required to follow command signals sent by transmission system operators (TSO), during power dispatching procedures. In this research, for sake of easy implementation and fine tuning linear controllers were augmented to deal with the inherent complexity of wind systems. However, an innovative control algorithm was incorporated into a linear controller to achieve the same effectiveness in performance under different operating points as complex controllers. In addition, a new linearization technique was developed to enhance approximation compared to conventional approaches. Numerous tests were conducted on a full variable speed wind system to validate power regulation and mitigation of oscillations concerning change in wind speed, and sag and swell voltage. The control indices of settling time, maximum overshoot and minimum undershoot in terms of which damping and performance are optimized were perceived to make a comprehensive assessment of the proposed approach. It is seen settling time for the three circumstances remained constant at a low value. Moreover, the controller either eliminated overshoot and undershoot or reduced these control properties acceptably. To sum, simulation results confirmed the proposed control method along with the new linearization technique were successful in the satisfaction of wind system requirements.

References

[1] T. Ackermann, Ed., "Wind Power in Power Systems," Apr. 2012.

[2] Fox, Jenkins, Flynn, O'Malley, Milborrow, Bryans, Anaya-Lara, and Watson, "Wind Power Integration: Connection and System Operational Aspects," May 2014.

[3] O. Anaya-Lara, N. Jenkins, J. Ekanayake, P. Cartwright, M. Hughes, "Wind Energy Generation: Modelling and Control", John Wiley & Sons, Chichester, 2009.

[4] S.M. Muyeen, J. Tamura, T. Murata, "Stability Augmentation of a Grid-connected Wind Farm," Green Energy and Technology, 2009.

[5] J. Laks and L. Pao, "Optimal Control of Wind Energy Systems: Towards a Global Approach (Munteanu, I. et al.; 2008) [Bookshelf]," IEEE Control Systems Magazine, vol. 29, no. 3, pp. 105–108, Jun. 2009.

[6] G. Rashid and M. H. Ali, "Nonlinear Control-Based Modified BFCL for LVRT Capacity Enhancement of DFIG-Based Wind Farm," IEEE Transactions on Energy Conversion, vol. 32, no. 1, pp. 284–295, Mar. 2017.

[7] X.-B. KONG and X.-J. LIU, "Nonlinear Model Predictive Control for DFIG-based Wind Power Generation," Acta Automatica Sinica, vol. 39, no. 5, pp. 636–643, Mar. 2014.

[8] J. Chen, L. Jiang, W. Yao, and Q. H. Wu, "Perturbation Estimation Based Nonlinear Adaptive Control of a Full-Rated Converter Wind Turbine for Fault Ride-Through Capability Enhancement," IEEE Transactions on Power Systems, vol. 29, no. 6, pp. 2733–2743, Nov. 2014.

[9] X.-B. KONG and X.-J. LIU, "Nonlinear Model Predictive Control for DFIG-based Wind Power Generation," Acta Automatica Sinica, vol. 39, no. 5, pp. 636–643, Mar. 2014.

[10] X. Liu, Y. Han, and C. Wang, " Second-order sliding mode control for power optimisation of DFIG-based variable speed wind turbine ," IET Renewable Power Generation, vol. 11, no. 2, pp. 408–418, Feb. 2017.

[11] S. M. Mozayan, M. Saad, H. Vahedi, H. Fortin-Blanchette, and M. Soltani, "Sliding Mode Control of PMSG Wind Turbine Based on Enhanced Exponential Reaching Law," IEEE Transactions on Industrial Electronics, vol. 63, no. 10, pp. 6148–6159, Oct. 2016.

[12] P. Xiong and D. Sun, "Backstepping-Based DPC Strategy of a Wind Turbine-Driven DFIG Under Normal and Harmonic Grid Voltage," IEEE Transactions on Power Electronics, vol. 31, no. 6, pp. 4216–4225, Jun. 2016.

[13] G.-D. Wang, R.-J. Wai, and Y. Liao, "Design of backstepping power control for grid-side converter of voltage source converter-based high-voltage dc wind power generation system," IET Renewable Power Generation, vol. 7, no. 2, pp. 118–133, Mar. 2013.

[14] L. Wang and M. Nguyen Thi, "Stability Enhancement of a PMSG-Based Offshore Wind Farm Fed to a Multi-Machine System Through an LCC-HVDC Link," IEEE Transactions on Power Systems, vol. 28, no. 3, pp. 3327–3334, Aug. 2013.

[15] L. Wang and D.-N. Truong, "Stability Enhancement of a Power System With a PMSG-Based and a DFIG-Based Offshore Wind Farm Using a SVC With an Adaptive-Network-Based Fuzzy Inference System," IEEE Transactions on Industrial Electronics, vol. 60, no. 7, pp. 2799–2807, Jul. 2013.

[16] A. Merabet, A. A. Tanvir, and K. Beddek, " Speed control of sensorless induction generator by artificial neural network in wind energy conversion system ," IET Renewable Power Generation, vol. 10, no. 10, pp. 1597–1606, Nov. 2016.

[17] F.-J. Lin, C.-H. Tsai, and K.-H. Tan, "Improved differential evolution-based Elman neural network controller for squirrel-cage induction generator system," IET Renewable Power Generation, vol. 10, no. 7, pp. 988–1001, Aug. 2016.

[18] W.-L. Chen and Y.-Y. Hsu, "Controller Design for an Induction Generator Driven by a Variable-Speed Wind Turbine," IEEE Transactions on Energy Conversion, vol. 21, no. 3, pp. 625–635, Sep. 2006.

[19] L. Wang and C.-T. Hsiung, "Dynamic Stability Improvement of an Integrated Grid-Connected Offshore Wind Farm and Marine-Current Farm Using a STATCOM," IEEE Transactions on Power Systems, vol. 26, no. 2, pp. 690–698, May 2011.

[20] S. M. Muyeen, R. Takahashi, T. Murata, and J. Tamura, "A Variable Speed Wind Turbine Control Strategy to Meet Wind Farm Grid Code Requirements," IEEE Transactions on Power Systems, vol. 25, no. 1, pp. 331–340, Feb. 2010.

[21] S. Masoud Barakati, Ali Mohammadi, Ebrahim Hojjati Najafabadi, Sajjad Farajianpour, Saeed Tavakoli, "New optimal linear control strategy for a variable speed wind energy conversion system," in Proceedings of 44th North America Power Symposium, IEEE press, pp. 1-6, September 2012.

[22] Leithead, W., Connor, B., Control of variable speed wind turbines: dynamic models, Int. J. Control, Vol. 73, No. 13, pp. 1173–1189, 2000.

[23] E. S. Abdin and W. Xu, "Control design and dynamic performance analysis of a wind turbine-induction generator unit," IEEE Transactions on Energy Conversion, vol. 15, no. 1, pp. 91–96, Mar. 2000.

[24] F. D. Bianchi, H. De Battista, R.J Mantz, "Wind Turbine Control Systems Principles: Modelling and Gain Scheduling Design", Springer-Verlag, London, 2007.

[25] T. Burton, N. Jenkins, D. Sharpe, and E. Bossanyi, "Wind Energy Handbook," May 2011.

[26] J. G. Slootweg, H. Polinder, and W. L. Kling, "Representing wind turbine electrical generating systems in fundamental frequency simulations," IEEE Transactions on Energy Conversion, vol. 18, no. 4, pp. 516–524, Dec. 2003.

[27] R. Vepa, "Nonlinear, Optimal Control of a Wind Turbine Generator," IEEE Transactions on Energy Conversion, vol. 26, no. 2, pp. 468–478, Jun. 2011.

[28] C. Nichita, D. Luca, B. Dakyo, and E. Ceanga, "Large band simulation of the wind speed for real time wind turbine simulators," 2003 IEEE Power Engineering Society General Meeting (IEEE Cat. No.03CH37491).

[29] Y. Petru, T. Thiringer, "Active Flicker Reduction from a Sea-based 2.5 MW Wind Park Connected to a Weak Grid", presented at the Nordic Workshop on Power Ind. Electron., Aalborg, Denmark, 2000.

[30] D. Grenier, L.-A. Dessaint, O. Akhrif, Y. Bonnassieux, and B. Le Pioufle, "Experimental nonlinear torque control of a permanent-magnet synchronous motor using saliency," IEEE Transactions on Industrial Electronics, vol. 44, no. 5, pp. 680–687, 1997.

[31] S. A. Papathanassiou and M. P. Papadopoulos, "Mechanical stresses in fixed-speed wind turbines due to network disturbances," IEEE Transactions on Energy Conversion, vol. 16, no. 4, pp. 361–367, 2001.

[32] S. A. Papathanassiou and M. P. Papadopoulos, "Dynamic behavior of variable speed wind turbines under stochastic wind," IEEE Transactions on Energy Conversion, vol. 14, no. 4, pp. 1617–1623, 1999.

[33] V. Akhmatov, " Analysis of dynamic behaviour of electric power systems with large amount of wind power", PhD Thesis, Technical University of Denmark, pp. 30–38, 2003.

[34] H. Nikkhajoei and R. Iravani, "Dynamic model and control of AC-DC-AC voltage-sourced converter system for distributed resources," 2008 IEEE Power and Energy Society General Meeting - Conversion and Delivery of Electrical Energy in the 21st Century, Jul. 2008.

[35] O. H. Bosgra, "Multivariable Feedback Control - Analysis and Design (Skogestad, S. and Postlewaite, I.; 2005) [book review]," IEEE Control Systems, vol. 27, no. 1, pp. 80–81, Feb. 2007.

[36] Ali Mohammadi, Saeed Tavakoli, S. Masoud Barakati, "On power tracking and alleviation by a new controller for fulfilment of the damping and performance requisites for a variable speed wind system: An optimal approach," *International Journal of Electrical and Power Energy Systems*, Vol. 75, pp. 187–193 (IF: 3.432), February 2016.